Biomedicine & Pharmacotherapy 180 (2024) 117517

Contents lists available at ScienceDirect

Biomedicine & Pharmacotherapy

journal homepage: www.elsevier.com/locate/biopha

Identification of nitrile-containing isoquinoline-related natural product derivatives as coronavirus entry inhibitors *in silico* and *in vitro*

Nasim Shahhamzehei [a], Sara Abdelfatah [a], Hannah S. Schwarzer-Sperber [b], Kathrin Sutter [b,c], Rümeysa Yücer [a], Gerhard Bringmann [d], Roland Schwarzer [c,*], Thomas Efferth [a,*]

[a] Department of Pharmaceutical Biology, Institute of Pharmaceutical and Biomedical Sciences, Johannes Gutenberg University, Staudinger Weg 5, Mainz 55128, Germany
[b] Institute for the Research on HIV and AIDS-Associated Diseases (HIV-AAD), University Hospital Essen, University Duisburg-Essen, Essen, Germany
[c] Institute for Virology, University Hospital Essen, University Duisburg-Essen, Essen, Germany
[d] Institute of Organic Chemistry, University of Würzburg, Am Hubland, Würzburg 97074, Germany

ARTICLE INFO

Keywords:
ACE2
SARS-CoV-2
Nitrile-containing natural product derivatives
Isoquinoline
Pan-entry inhibitor
Virtual drug screening

ABSTRACT

Severe acute respiratory syndrome coronavirus 2 (SARS-CoV-2) has caused millions of infections and deaths worldwide since its emergence in Wuhan, China, in late 2019. Natural product inhibitors targeting the interaction between the receptor-binding domain (RBD) of the SARS-CoV-2 spike protein and human angiotensin-converting enzyme 2 (ACE2), crucial for viral attachment and cellular entry, are of significant interest as potential antiviral agents. In this study a library of nitrile- and sulfur-containing natural product derived compounds were used for virtual drug screening against the RBD of the SARS-CoV-2 spike protein. The top 18 compounds from docking were tested for their efficacy to inhibit virus entry. In vitro experiments revealed that compounds **9**, **14**, and **15** inhibited SARS-CoV-2 pseudovirus and live virus entry in HEK-ACE2 and Vero E6 host cells at low micromolar IC_{50} values. Cell viability assays showed these compounds exerted low cytotoxicity towards MRC5, Vero E6, and HEK-ACE2 cell lines. Microscale thermophoresis revealed all three compounds strongly bound to the RBDs of SARS-CoV-2, SARS-CoV-2 XBB, SARS-CoV-1, MERS-CoV, and HCoV-HKU1, with their K_d values increasing as RBD sequence similarity decreased. Molecular docking studies indicated compounds **9**, **14**, and **15** bound to the SARS-CoV-2 spike protein RBD and interacted with hotspot amino acid residues required for the RBD-ACE2 interaction and cellular infection. These three nitrile-containing candidates, particularly compound **15**, should be considered for further development as potential pan-coronavirus entry inhibitors.

1. Introduction

The COVID-19 (coronavirus disease 2019) pandemic caused by the severe acute respiratory syndrome coronavirus 2 (SARS-CoV-2) has infected more than 774 million individuals with more than 7 million deaths by the end of June 2024 (https://covid19.who.int/). In addition, this pandemic provoked an impending economic crisis and recession on a global scale [1]. Despite the development of successful vaccinations, antigenic mutations can result in immune evasion in convalescent COVID-19 patients and vaccines, which can cause infection, hospitalization, and even death [2]. Today, remdesivir [3] and molnupiravir, targeting RNA-dependent RNA polymerase, and nirmatrelvir/ritonavir, targeting the main protease (M^{pro}) are approved by the United States Food and Drug Administration (US FDA) for the treatment of COVID-19 in certain adults [4], but no small molecule has so far been approved to target the spike protein, which is a trimeric protein located on the surface of the viruses. The spike protein is one of the most important targets, since its inhibition prevents the entry of the virus into the host cells and thereby inhibits virus replication. Although the use of monoclonal antibodies (mAb), that target the spike protein, can be an alternative strategy to disrupt early events in the SARS-CoV-2 life cycle, there are novel SARS-CoV-2 variants evading mAb-induced protection [5]. Furthermore, issues with the solubility, immunogenicity, and appropriateness of the antibodies for oral or inhaled delivery pose challenges [6]. The spike protein has a full length of 1273 amino acids, including the N-terminus signal peptide, the S1 subunit, and the S2 subunit. S1 includes the N-terminal domain (NTD), the receptor-binding domain (RBD), and two C-terminal domains (CTD1 and CTD2), while S2

* Corresponding authors.
E-mail addresses: Roland.Schwarzer@uk-essen.de (R. Schwarzer), efferth@uni-mainz.de (T. Efferth).

https://doi.org/10.1016/j.biopha.2024.117517
Received 11 July 2024; Received in revised form 25 September 2024; Accepted 26 September 2024
Available online 1 October 2024

includes fusion peptide (FP), fusion-peptide proximal region (FPPR), heptad repeat 1 (HR1), central helix (CH), connector domain (CD), heptad repeat 2 (HR2), transmembrane segment (TM), and the cytoplasmic tail (CT). The receptor binding domain (RBD) contains two subdomains: a five-stranded antiparallel β-sheet connected by short helices and loops, and an extended loop, named receptor binding motif (RBM). The spike protein can bind to two or three host ACE2 molecules through the RBD [7], which makes it a promising target for drug development. Molecules containing sulfur are frequently found in nature. They are active both pharmacologically and physiologically and show vast anticancer, antiviral, antibacterial, and antifungal activities [8–10]. Nitrile-containing compounds can be found in a variety of organisms, including bacteria, fungi, plants, insects, sponges, and other aquatic creatures, and have a wide range of pharmacological activities, including anti-microbial, anti-cancer, anti-inflammatory, and antioxidant properties [11–13]. During the past decades, both nitrile- and sulfur-containing compounds have reached increasing importance in medicinal chemistry, thus attracting our attention to the development of pan-coronaviral inhibitors.

In this study, our aim was to explore natural pan-coronaviral inhibitors, focusing on sulfur- and nitrile-containing compounds, against different spike proteins of the coronavirus family. For this purpose, we studied 143 sulfur- and nitrile-containing compounds from the ZINC database and from the literature.

2. Materials and methods

2.1. Cell lines

HEK-ACE2 cells were obtained from ATCC (American Type Culture Collection, Virginia, USA). The 293T cell line was kindly provided by Dr. Helen May-Simera (Institute of Molecular Physiology, Johannes Gutenberg University, Mainz, Germany). They were grown in Dulbecco's Modified Eagle Medium (DMEM; Thermo Fisher) supplemented with 10 % fetal bovine serum (FBS) and 1 % penicillin/streptomycin (P/S). MRC-5 lung fibroblasts were obtained from Dr. Sebastian Zahnreich (Department of Radiation Oncology and Radiation Therapy, University Medical Centre of the Johannes Gutenberg University, Mainz, Germany) and grown in DMEM, low glucose, pyruvate medium with 15 % FBS, 1 % P/S, and 1 % MEM. Non-essential amino acids (Thermo Fisher) were used for cultivation. Vero E6 cells were obtained from ATCC and cultured in DMEM supplemented with 10 % FBS, 1 % L-glutamine (Capricorn Scientific, Germany), and 1 % P/S. All cell lines were incubated in a humidified atmosphere at 37 °C and 5 % CO_2.

2.2. Compounds

The chemical structures of 143 natural-derived nitrile- and sulfur-containing compounds were downloaded from the ZINC and PubChem databases in the three-dimensional SDF format. Based on *in silico* studies, 18 selected compounds were provided by Vitas-M Laboratory (Hong Kong, China). The compounds had a guaranteed purity of > 90 %. Based on the ^{1}H NMR spectra given by the provider, the purity of most of the compounds was higher, usually > 95 %. All compounds were dissolved in DMSO at a concentration of 20 mM and stored at − 20 °C.

2.3. Virtual screening

In this study, AutoDock Vina in PyRx 0.8 software was used for the virtual screening of 143 natural-derived compounds from the ZINC database and from the literature (blind docking mode). As a target, the RBD domain of the spike protein of SARS-CoV-2 (PDB ID: 7bnn) was chosen to identify compounds with high a affinity and low a binding energy (kcal/mol). For validation and verification of PyRx results, the top 84 compounds, with a cut-off value of − 6 kcal/mol, were subjected to AutoDock 4.2.6 (defined docking mode) to identify their binding affinity for the RBD domain of the spike protein of SARS-CoV-2 (PDB ID: 7bnn) using the Lamarckian algorithm. The protein was kept rigid, while the ligand moved during the docking simulation. The parameters were set to 250 runs and 2,500,000 energy evaluations for each cycle, while the other docking parameters were kept at default values as described by our group [14]. Docking was conducted using the high-performance supercomputer MOGON (Johannes Gutenberg University, Mainz, Germany). The AutoDock version 1.5.6 was used to convert the Protein Data Bank file of target proteins (PDB) to PDBQT files and create a grid box. The energy of the compounds was minimized and converted from SDF format to PDBQT format using the PyRx software.

2.4. Plasmids

For production of pseudovirus plasmids: pHAGE-CMV-Luc2-IRES-ZsGreen-W (BEI Cat. # NR-52516), HDM-Hgpm2 (BEI Cat. # NR-52517), HDM-tat1b (BEI Cat. # NR-52518), pRC-CMV-Rev1b (BEI Cat. # NR-52519), and HDM-IDTSpike-fixK-HA-tail (BEI Cat. # NR-53765) were obtained from BEI Resources (US). In order to generate a working stock, all plasmids were amplified in *Escherichia coli* using One Shot™ TOP10 chemically competent *E. coli* (Invitrogen, Thermo Fisher). They were extracted and purified using the Plasmid Plus Maxi Kit (QIAGEN).

2.5. Production of SARS-CoV-2 pseudoviruses and titration

293T cells were seeded in DMEM medium containing 10 % FBS so that they were 70–80 % confluent the next day. Twenty-four hours after seeding, the cells were transfected with 1 μg of the Luciferase IRES ZsGreen (NR-52516) backbone, 0.22 μg each of the plasmids HDM-Hgpm2 (NR-52517), pRC-CMV-Rev1b (NR-52519), and HDM-tat1b (NR-52518) with or without 0.34 μg SARS-CoV-2 spike (NR-53765) as a negative control using Lipofectamine™ 2000 transfection reagent (Invitrogen, Thermo Fisher). Eighteen hours after transfection, the medium was changed with fresh medium, 48 and 72 h after transfection, the supernatant was collected, centrifuged for 3 min at 1250 rpm, and stored at − 80 °C. For the titration of pseudoviruses, HEK-ACE2 was seeded (12.5×10^3 cells/well) in white 96-well plates (Greiner, Cat. # 655074). Twenty-four hours after seeding, a serial dilution of spike-pseudotyped Luciferase IRES ZsGreen virus was prepared. Starting with an undiluted virus, six 1:2 dilutions were made. Twenty-four hours after infection, cell supernatants were replaced with 50 μl fresh medium for each sample. Then, 50 μl Bright-Glo Luciferase Assay reagent (Promega, E2610) were added per well, and cells were incubated for 2 min at room temperature. Luciferase activities were measured using an Infinite M2000™ Pro plate reader (Tecan, Crailsheim, Germany). The measured luciferase activity, defined as relative light unit (RLU) *vs.* virus dilution, were plotted, and the amount of pseudovirus was selected for further assays, which has sufficient (> 1000-fold) signal intensity above the virus-only background and in the linear part of the curve [15,16].

2.6. Pseudovirus inhibition assay

HEK-ACE2 (12.5×10^3cells/well) were seeded in the white 96-well plate (Greiner, Cat. # 655074) 1 d before infection. The next day, the pseudoviruses were incubated at 37 °C for 1.5 h with either 30 μM of the compounds or DMSO, before being added to the cells. Twenty-four hours after infection, the medium was discarded, and 50 μl of fresh medium were added to each well, followed by 50 μl of Bright-Glo Luciferase reagent (Promega, E2610) and incubated for 2 min in the dark at room temperature. The luminescence was measured using an Infinite M2000 Pro™ plate reader (Tecan) without attenuation and a luminescence integration time of 1 s. As a next step, compounds exhibiting more than 50 % inhibitory activity at a fixed concentration of 30 μM were selected for dose-response studies in a concentration range from 0 to 30 μM in all experiments. Etravirine was used as a positive control [17]. To calculate

the percentage of infection, the following equation was used: % infection = [(mean RLU from each sample (virus + compound) - mean RLU from negative cell control/(mean RLU from virus control – mean RLU from negative cell control) × 100]. The percentage of infection vs. the log concentration of the inhibitors was used to calculate the IC_{50} values [15,16]. As a confirmatory assay, fluorescence microscopy was performed. HEK-ACE2 (10×10^3 cells/well) were seeded in black 96-well plates (Greiner, Cat.# 655936) 1 d before infection. The next day, before the infection pseudoviruses were incubated for 1.5 h at 37 °C in the presence of 5 μM test compounds or DMSO. Seventy-two hours after infection, GFP fluorescence quantified using live imaging system, results were analyzed using ImageJ.

2.7. SARS-CoV-2 propagation and quantification

A SARS-CoV-2 isolate (referred to as the Essen isolate) derived from patient material was used for infection experiments as previously described [18]. The virus was produced in Vero E6 cells, plated at a concentration of 2×10^6 Vero E6 cells in a T75 flask, and incubated for 24 h at 37 °C with 5 % CO_2 in DMEM supplemented with 10 % FBS, 1 % L-glutamine, 1 % penicillin, and 1 % streptomycin. The cells were then exposed to the isolated virus and incubated for an additional 72 h. The culture supernatant was then clarified by centrifugation and stored at − 80 °C. Viral concentrations were assessed using an endpoint dilution assay to determine the 50 % tissue culture infective dose ($TCID_{50}$).

2.8. SARS-CoV-2 in-cell ELISA procedure

Virus infections were quantified by in-cell ELISA following a recently published protocol [19]: A total of 2×10^4 cells/well were seeded in a flat-bottom 96-well plate 1 d prior to infection. The cells were then infected with SARS-CoV-2 for 24 h and subsequently fixed using 4 % paraformaldehyde in phosphate buffered saline (PBS). Permeabilization was conducted using a 1 % Triton-X-100 solution in PBS, followed by blocking with 3 % fetal calf serum (FCS) in PBS. Next, the primary antibody (anti-N mAb1 ABIN6952435, Antibodies Online, Aachen, Germany) was added and incubated for 2 h at room temperature. Subsequently, a peroxidase-labeled secondary antibody (Cat. # 115-035-003, Jackson Immuno Research, Cambridge, UK) was applied for an additional hour, followed by washing steps with a solution of 0.05 % Tween-20 in PBS. Finally, tetramethylbenzidine (TMB) substrate was added, and the enzymatic reaction was terminated using 0.5 M HCl. The absorbance of the dye was then measured at 450 nm using a Spark® 10 M multimode microplate reader (Tecan).

2.9. Cell viability assay

Cell viability was measured using the resazurin assay as previously described [20]. Human diploid MRC-5 lung fibroblasts and human embryonic kidney HEK-ACE2 cells were seeded (2×10^4 cells/well and 1×10^4, respectively) into 96-well culture plates and incubated overnight before treatment. On the second day, the cells were treated with ten concentrations of compounds in a range of 0.3–100 μM. After 24 h of incubation, 20 μl of 0.01 % resazurin (Promega, Mannheim, Germany) were added to each well. The fluorescence was detected after 4 h of incubation using an Infinite M2000™ Pro plate reader (Tecan) at Ex/Em = 550 nm/590 nm wavelength. The cell viability was calculated in comparison to the DMSO control. The DMSO final concentration was 0.5 %. The 50 % cytotoxicity concentration (CC_{50}) values were calculated in comparison to the DMSO-treated control. Each experiment was independently repeated three times, with six wells for each concentration. For the Vero E6 cell line, a total of 20×10^3 cells per well were seeded into 96-well culture plates and incubated overnight. On the second day, the cells were treated with a wide range of concentrations of compounds. After 24 h, the supernatants were replaced with 100 μl of fresh medium for each sample. Then, 20 μl of CellTiter-Blue™ reagent (Promega, Madison, USA) were added per well, and cells were incubated for 4 h at 37 °C with 5 % CO_2. Colorimetric analysis of treated cells was done with a Spark® 10 M multimode microplate reader (Tecan) detecting fluorescence with an excitation of 560 nm and an emission at 590 nm.

2.10. Sequence alignment

The full length of amino acid sequences of the RBD domain of the spike protein of SARS-CoV-2 (P0DTC2), SARS-CoV-1 (P59594), MERS-CoV (K9N5Q8), and HCoV-HKU1 (Q0ZME7) were accessed from the UniProt database, and for SARS-CoV-2 XBB.1. The sequences were downloaded from the Protein Data Bank (PDB ID: 8iou), and then the sequence alignment was performed using Clustal Omega (EMBL-EBI, Wellcome Genome Campus, Hinxton, Cambridgeshire, UK), and the figures were prepared using Jalviwe 2.11.3.2 (University of Dundee, Scotland, UK).

2.11. Microscale thermophoresis

The recombinant RBD of spike proteins of SARS-CoV-2, SARS-CoV-2 XBB.1, SARS-CoV-1, MERS-CoV, and HCoV-HKU1 were purchased from Bio-Techne (Wiesbaden, Germany) to perform microscale thermophoresis (MST), following previously established protocols [21,22]. Briefly, the recombinant proteins were labeled with the Monolith Protein Labeling Kit RED-NNHS 2nd Generation (MO-L011, Nano Temper Technologies GmbH, Munich, Germany) according to the manufacturer's instructions. The final protein concentrations after labeling were 1500 nM, 1500 nM, 1000 nM, 750 nM, and 1500 nM (Nanodrop, Thermo Fisher Scientific) for recombinant RBD of SARS-CoV-2, SARS-CoV-2 XBB.1, SARS-CoV-1, MERS-CoV, and HCoV-HKU1, respectively. Titration was performed using 16 serial dilutions, ranging from 200 to 0.006 M concentration (dilution steps 1:1). Ligand and protein were incubated for 30 min at room temperature in assay buffer (50 mM Tris buffer (pH 7.4) containing 10 mM $MgCl_2$, 150 mM NaCl, and 0.05 % Tween-20). Measurements were carried out in Monolith NT.115 standard capillaries (MO-K022, Nano Temper Technologies GmbH, Munich, Germany). The laser power was adjusted to 10 %, 20 %, 40 %, and 60 %, and the LED (light-emitting diodes) power was 20 % for SARS-CoV-2, SARS-CoV-1, MERS-CoV, HCoV-HKU1, and 30 % for SARS-CoV-2 XBB.1. Signals were measured using the Monolith NT.115 instrument (Nano Temper Technologies). Fitting curves and K_d values were calculated using NT Analysis 1.5.41. software (Nano Temper Technologies).

2.12. Molecular docking

The top compounds obtained from *in vitro* experiments were rescreened against RBD of the spike protein of SARS-CoV-2 (PDB ID: 7bnn), SARS-CoV-2 XBB.1(PDB ID: 8iou), SARS-CoV-1 (PDB ID: 6acd), MERS-CoV (PDB ID: 6nb03), and HCoV-HKU1 (PDB ID: 8opo) using AutoDock 4.2.6 (defined docking mode) in order to identify not only their binding affinity for different coronavirus RBD, but also the amino acid residues involved in the binding site. Docking was conducted using the high-performance supercomputer MOGON (Johannes Gutenberg University, Mainz, Germany). The visualization and imaging were created by Discovery Studio Visualizer V 21.1.0.20298 (San Diego, California, United States).

2.13. Statistics and data fitting

All inhibition assays were performed at least as duplicates per plate, and all results shown are the average of at least three independent experiments. The binding data were converted to percent infection and fitted with standard log inhibitor *vs.* normalized response models (four parameters) using nonlinear regression in GraphPad Prism 8 (GraphPad, La Jolla, CA, USA) to establish half-maximal toxicity or inhibitory

concentrations (CC_{50}, IC_{50}). The selectivity index (SI) of active compounds was calculated using the $SI = CC_{50} / EC_{50}$ equation for live and pseudo-typed viruses. The correlation between the K_d values and pecentage of identity of RBDs was calculated using the Pearson correlation tes.

3. Results

3.1. Virtual screening

Starting from a ZINC library of 97 natural-derived compounds and a library of 46 natural compounds preselected from the literature, virtual screening was performed with PyRx. A total of 84 compounds were selected based on their lowest PyRx-based binding energies (cut-off value: − 6 kcal/mol) to the RBD of the SARS-CoV-2 spike protein. For further evaluation and validation, they were subjected to AutoDock 4.2.6. Based on the lowest binding energy (cut-off value: − 7 kcal/mol), 18 candidates were selected for the *in vitro* experiments, and etravirine was used as a positive control, see Table 1. The structures of top 18 compounds are shown in Fig. 1.

3.2. Development of a SARS-CoV-2 pseudovirus assay

Our goal was to develop a sensitive SARS-CoV-2 neutralization assay by introducing SARS-CoV-2 spike protein into lentiviruses to evaluate inhibition of viral entry. The 293 T cell line was co-transfected with the plasmids and the supernatant was harvested 72 h later, which was then used to infect the HEK-ACE2 cells. Measuring the titers of the produced pseudoviruses was based on luminescence signal reads obtained from the activity of the expressed luciferase. The right titer of the generated pseudoviruses was selected as the dilution that results in an RLU above bald pseudovirus as a negative control and in the linear part of the curve (10^4–5×10^5) (Fig. 2A). In our case, 5×10^5 RLU/well were used to maximize the use of each lot of the produced pseudoviruses, and it worked very well in neutralization assays.

3.3. Inhibition of pseudotyped SARS-CoV-2 infection

Luciferase assays were performed in HEK-ACE2 cells to screen the 18 top candidates selected from the in silico studies to find novel anti-SARS-COV-2 entry inhibitors. After the preliminary screening (Fig. 2B), three compounds inhibited pseudovirus entry, substances **9**, **14**, and **15**. Notably, all three compounds contained a nitrile group. These three compounds were then subjected to dose-response experiments in order to calculate the concentration of each compound required to inhibit pseudovirus entry by half (IC_{50}). The IC_{50} values for compounds **9**, **14**, and **15** were 1.061 ± 0.08, 3.87 ± 0.28, and 1.85 ± 0.37 μM, respectively (Fig. 2C). GFP fluorescence measured from live fluorescence microscopy demonstrated that compound **9** strongly protected the cells from pseudovirus infection, while compound **15** had moderate and

Table 1
PyRx and molecular docking results of 18 natural-derived selected compounds and etravirine as a positive control binding to the RBD of spike protein of SARS-CoV-2 (PDB ID: 7bnn).

Compound number	ZINC-ID	Compound-IUPAC name	PyRx binding energy (kcal/mol)	AutoDock binding energy (kcal/mol)	Ki (μM)
Compound **1**	ZINC000002092410	Ethyl 2-{[(6-bromo-2-oxo-2H-chromen-3-yl)carbonyl]amino}-4,5,6,7,8,9,10,11,12,13-decahydrocyclododeca[*b*]thiophene-3-carboxylate	− 7.80	− 9.16 ± 0.03	0.193 ± 0.01
Compound **2**	ZINC000247984074	Ethyl (1R,2R,9R,12S)-6-(furan-2-carbonylamino)-16-methoxy-9-methyl-5-thiapentacyclo[10.8.0.02,9.04,8.013,18]icosa-4(8),6,13(18),14,16-pentaene-7-carboxylate	− 6.90	− 8.88 ± 0.16	0.32 ± 0.08
Compound **3**	ZINC000002060195	N-(3-cyano-4,5-diphenylfuran-2-yl)-2-(4-methoxyphenyl)acetamide325739–78–4	− 7.90	− 8.65 ± 0.004	0.45 ± 0.005
Compound **4**	ZINC000000568457	Methyl 5-[(1,3-benzodioxol-5-ylcarbonyl)amino]-4-cyano-3 methylthiophene-2-carboxylate	− 6.30	− 8.33 ± 0.009	0.77 ± 0.01
Compound **5**	ZINC000000846863	Ethyl 5-acetyl-4-methyl-2-({[(4-methyl-2-oxo-2H-chromen-7-yl)oxy]acetyl}amino)thiophene-3-carboxylate	− 7.20	− 8.27 ± 0.20	0.91 ± 0.27
Compound **6**	ZINC000001061006	N-(3-cyano-4,5-dimethylthiophen-2-yl)-2-((4-methyl-2-oxo-2H-chromen-7-yl)oxy) acetamide	− 6.40	− 7.87 ± 0.15	1.75 ± 0.39
Compound **7**	ZINC000000846827	Diethyl 3-methyl-5-{[(2*E*)-3-phenylprop-2-enoyl]amino}thiophene-2,4-dicarboxylate	− 6.30	− 7.84 ± 0.07	1.81 ± 0.23
Compound **8**	ZINC000100778515	4-imino-2-(6-methoxy-4-oxo-4H-chromen-3-yl)−6,7-dihydro-4H-[1,3]dioxolo [4,5-*g*]pyrido[2,1-*a*]isoquinoline-3-carbonitrile	− 8.30	− 7.82 ± 0.004	1.86 ± 0.008
Compound **9**	ZINC000101140820	4-imino-2-[3-methoxy-4-(propan-2-yloxy)phenyl]-6,7,11,12-tetrahydro-4H,10H-[1,4]dioxepino[2,3-*g*]pyrido[2,1-*a*]isoquinoline-3-carbonitrile	− 8.00	− 7.80 ± 0.01	1.91 ± 0.04
Compound **10**	ZINC000000037324	N-[4-(cyanomethyl)phenyl]-2-(4-methoxyphenyl)acetamide	− 6.30	− 7.68 ± 0.009	2.35 ± 0.02
Compound **11**	ZINC000101374185	2-(4-hydroxy-3-methoxyphenyl)-4-imino-9,10-dimethoxy-6,7-dihydro-4H-pyrido [2,1-*a*]isoquinoline-3-carbonitrile	− 6.50	− 7.67 ± 0.02	2.82 ± 0.08
Compound **12**	ZINC000001965160	Ethyl 4-cyano-5-(3,5-dimethoxybenzamido)-3-methylthiophene-2-carboxylate	− 6.00	− 7.52 ± 0.23	3.3 ± 1.09
Compound **13**	ZINC000000626395	2,4-diethyl 3-methyl-5-{2-[(4-methyl-2-oxo-2H-chromen-7-yl)oxy]acetamido} thiophene-2,4-dicarboxylate	− 7.00	− 7.48 ± 0.02	3.31 ± 0.14
Compound **14**	ZINC000100778854	4-imino-2-(3-methoxyphenyl)-6,7-dihydro-4H-[1,3]dioxolo[4,5-*g*]pyrido[2,1-*a*] isoquinoline-3-carbonitrile	− 8.00	− 7.34 ± 0.004	4.17 ± 0.01
Compound **15**	ZINC000101345860	2-(1,3-benzodioxol-5-yl)-4-imino-9,10-dimethoxy-6,7-dihydro-4H-pyrido[2,1-*a*] isoquinoline-3-carbonitrile	− 7.20	− 7.33 ± 0.10	4.33 ± 0.80
Compound **16**	ZINC000100779013	Methyl 4-(3-cyano-4-imino-6,7-dihydro-4H-[1,3]dioxolo[4,5-*g*]pyrido[2,1-*a*] isoquinolin-2-yl)benzoate	− 8.30	− 7.23 ± 0.02	4.9 ± 0.24
Compound **17**	ZINC000253412567	N~2~-[(7*S*)-7-(acetylamino)-1,2,3-trimethoxy-9-oxo-5,6,7,9-tetrahydrobenzo[*a*] heptalen-10-yl]-N-(2-hydroxyethyl)-L-methioninamide	− 6.40	− 7.05 ± 0.38	5.42 ± 1.53
Compound **18**	ZINC000005225262	Ethyl 2-[[2-[(2S)-2-benzamido-4-methylpentanoyl]oxyacetyl]amino]-5,6-dihydro-4H-cyclopenta[*b*]thiophene-3-carboxylate	− 6.3	− 7.01 ± 0.50	4.96 ± 1.45
Etravirine (positive control)	ZINC000000602632	4-[6-amino-5-bromo-2-(4-cyanoanilino)pyrimidin-4-yl]oxy-3,5-dimethylbenzonitrile	− 6.70	− 7.34 ± 0.02	4.15 ± 0.16

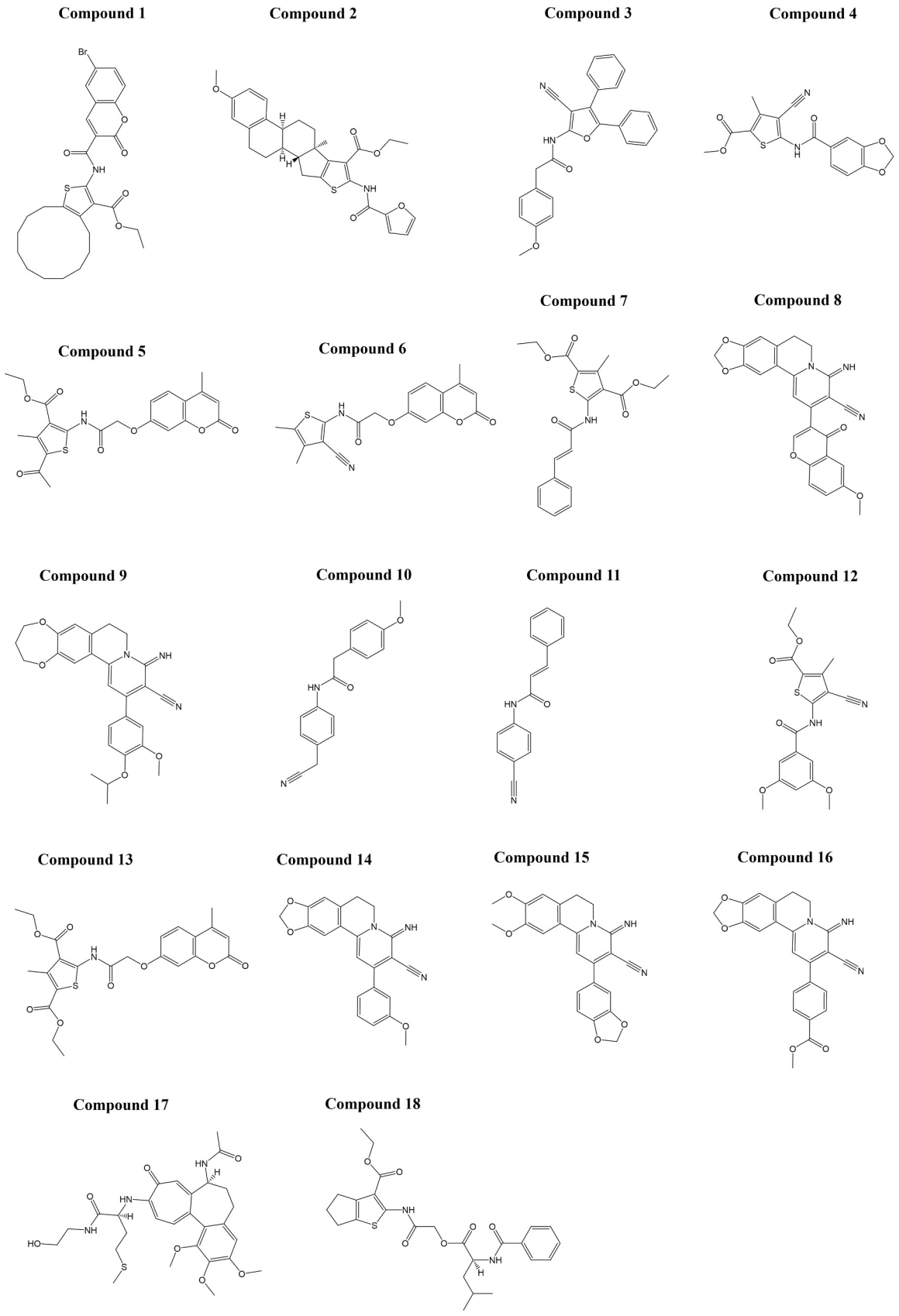

Fig. 1. Chemical structures of the top 18 natural-derived compounds exhibiting the lowest binding energy to the RBD of the SARS-CoV-2 spike protein.

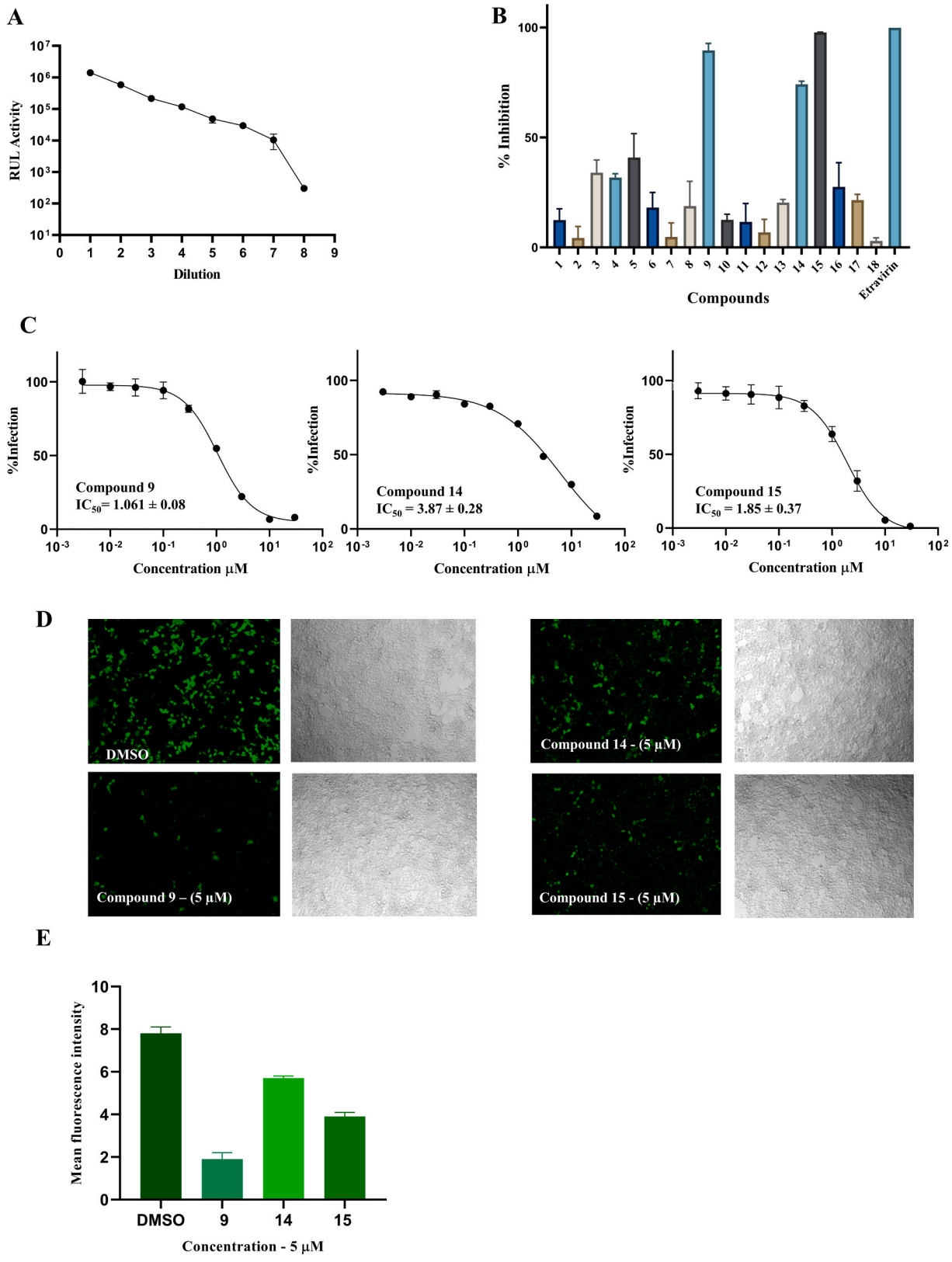

Fig. 2. Identification of entry inhibitors against pseudotyped SARS-CoV-2 lentivirus in HEK-ACE2 cells: A) Titration of the SARS-CoV-2 pseudovirus. Samples were run in duplicates, and the data are shown as mean ± SD. B) Percentage of inhibition of the SARS-CoV-2 pseudovirus in the presence of 18 selected natural-derived compounds and etravirine as a positive control (30 μM). C) Dose-response curves of compounds **9**, **14**, and **15** on the SARS-CoV-2 pseudovirus, IC_{50} values and data points are shown as mean ± SD for three independent replicates. D) fluorescence microscopic images of HEK-ACE2 treated with pseudotyped SARS-CoV-2 lentivirus in the presence of 5 μM of compounds **9**, **14**, and **15**. E) quantification of GFP fluoresces standardized to the mean of fluorescence intensity using Image J, at 5 μM concentration and presented as mean ± S.D of three replicates.

compound **14** had only week effects, which was consistent with the results from the luciferase inhibition assay (Fig. 2D).

3.4. Inhibition of live SARS-CoV-2 replication

The inhibitory activity of compounds **9**, **14**, and **15** towards the live SARS-CoV-2 viruses were assessed in titration experiments in order to calculate the IC_{50} values. Compound **15** effectively blocked SARS-CoV-2 infection at the cellular level with an IC_{50} of 9.32 ± 1.3 μM. Compounds **9** and **14** also showed inhibiting effects against SARS-CoV-2, with IC_{50} values of 22.86 ± 4.3 μM and 26.26 ± 7.38 μM, respectively (Fig. 3).

3.5. Cell viability assay

The cytotoxicity of compounds **9**, **14**, and **15** was tested on human MRC-5 fibroblasts, HEK-ACE2 cells, and Vero E6 cells using the resazurin assay. Compound **9** was cytotoxic towards HEK-ACE2, human MRC-5 fibroblasts, and Vero E6 cells with CC_{50} values of 28.29 ± 1.2, 81.15 ± 0.36, and 99.7 ± 1.5 μM, respectively. Compound **14** was cytotoxic against HEK-ACE2 and Vero E6 cells with CC_{50} values of 38.7 ± 1.5 and 96.8 ± 1.5, respectively, while it did not show toxicity against human MRC-5 fibroblasts. While compound **15** was cytotoxic against HEK-ACE2, with a CC_{50} value of 23.31 ± 3.06 μM, it did not display toxic effects towards human MRC-5 fibroblasts and Vero E6 cells (Fig. 4).

3.6. Sequence alignment

To determine whether our top compounds can bind to the spike protein of various coronavirus family members, sequence alignments were performed to identify the similarity between the receptor-binding domains (RBD) of the spike proteins from different coronavirus family members. The results revealed 89.91 %, 73.42 %, 18.75 %, and 19.81 % identity of the SARS-CoV-2 spike RBD domain to SARS-CoV-2 XBB.1 (Omicron variant), SARS-CoV-1, MERS-CoV, and HCoV-HKU1, respectively. Fig. 5 shows the conserved amino acid residues between the RBD domain of the spike protein of coronaviruses. The dark blue color indicates > 80 % identity, the blue color stands for > 60 %, and the light blue color means > 40 %.

3.7. Microscale thermophoresis

Microscale thermophoresis as a sensitive technology was performed to determine the binding affinity between active compounds and labeled RBD of the spike proteins from different coronavirus species, including different SARS-CoV-2 variants, SARS-CoV-1 and MERS, as well as the endemic strain HCoV-HKU1. For this purpose, the labeled recombinant RBDs of the spike proteins of SARS-CoV-2, SRAS-CoV-2 XBB.1, SARS-CoV-1, MERS-CoV, and HCoV-HKU1 were titrated against different concentrations of selected compounds. Compound **9** was bound to the RBD of spike protein of SARS-CoV-2, SARS-CoV-2 XBB.1, SARS-CoV-1, HCoV-HKU1, and MERS-CoV, with K_d values of 1.38, 3.7, 20.8, 23.3, and 23.3 μM, respectively. Compound **14** was bound to the spike protein of SARS-CoV-2, SARS-CoV-2 XBB.1, SARS-CoV-1, HCoV-HKU1, and MERS-CoV, with K_d values of 1.29, 1.39, 41.5, 50.1, and 63.1 μM, respectively. Finally, compound **15** resulted in K_d values of 1.4, 5.1, 28.4, and 48.3 μM for the spike protein of SARS-CoV-2, SARS-CoV-2 XBB.1, SARS-CoV-1, HCoV-HKU1, and MERS-CoV, respectively (Fig. 6).

3.8. Binding mode of the top candidates

Molecular docking with AutoDock 4.2.6 revealed high binding affinities of compounds **9**, **14**, and **15** to the RBD of spike proteins of SARS-CoV-2, SARS-CoV-2 XBB.1, SARS-CoV-1, MERS-CoV, and HCoV-HKU1, which can block the binding of RBD and ACE2 and thus protect healthy cells and prevent further degeneration in the early stage of infection. The three candidate compounds showed lowest binding energy (LBE) values between − 6.21 and − 8.11 kcal/mol and predicted inhibition constants (pK_i) between 28.22 and 1.14 μM. The amino acid interactions between the three candidate compounds and the proteins of interest are displayed in Fig. 7.

4. Discussion

Up to now, three zoonotic coronaviruses (CoVs) have been identified that cause deadly pneumonia outbreaks in humans, thereby posing a significant threat to public health. The SARS-CoV-1 caused severe acute respiratory syndrome (SARS) first appeared in 2002 and quickly expanded to five continents. MERS-CoV caused the Middle East respiratory syndrome (MERS), leading to high fatality rates at the Arabic peninsula in 2012, and the severe acute respiratory syndrome coronavirus 2 (SARS-CoV-2) rapidly developed to a global pandemic [23].

Several vaccines and antiviral medications have been developed to combat the COVID-19 pandemic. However, the diverse SARS-CoV-2 variants of concern (VOCs), especially Omicron and its sub-lineages, made the current COVID-19 vaccines and therapeutic antibodies less effective [24]. Along with SARS-CoV-2 and MERS-CoV, the four seasonal endemic HCoVs (OC43, HKU1, 229E, and NL63) still cause disease in humans [25]. Moreover, new studies showed that some SARS-related coronaviruses (SARSr-CoVs) in bats have the potential to cause novel coronavirus diseases in humans. Given these facts, a pan-coronavirus (pan-CoV) drug should be developed to prevent infection not only with SARS-CoV-2 and its variants but also with other newly emerging or reemerging HCoVs [26].

From 2010 to 2020, the US FDA has granted approval to at least one medicine containing a nitrile group every year [27]. These

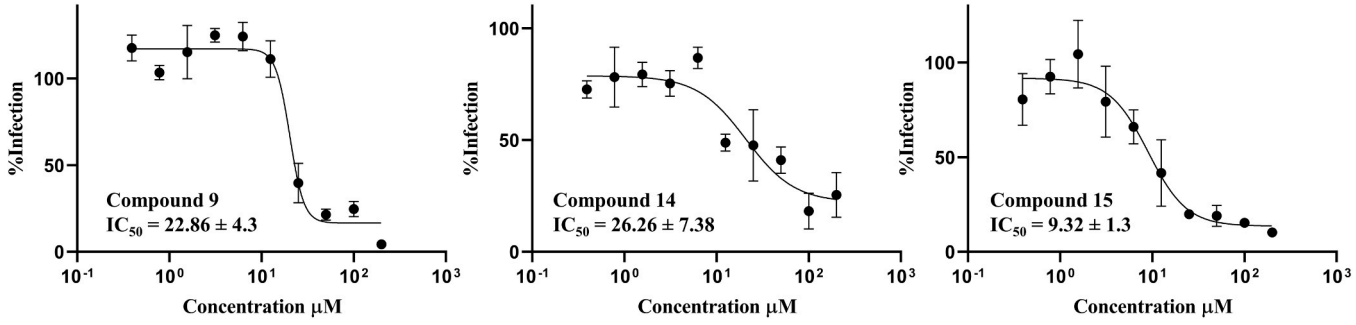

Fig. 3. Inhibition of fully replication-competent SARS-CoV-2. Vero E6 cells were infected with a clinical SARS-CoV-2 isolate for 24 h in the presence of different candidate inhibitors at the indicated concentrations. Infection levels were quantified by in-cell ELISA and normalized to mock-treated control wells (infected, but non-treated). Infection data were fitted with a four parameters inhibitor vs. response function (Y = Bottom + (Top - Bottom)/(1 + (IC_{50} / X) ^ HillSlope) using the statistics software GraphPad prism. Data points show mean ± standard error of the mean, calculated from at least three independent titrations of each compound.

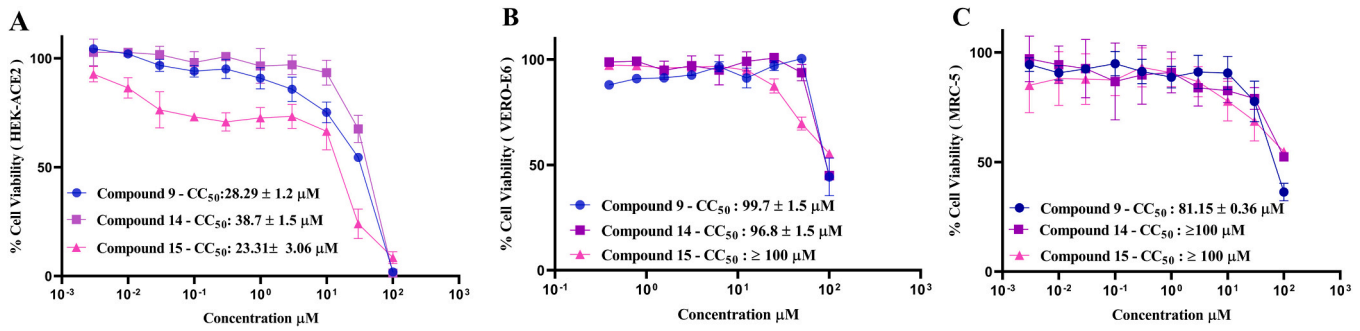

Fig. 4. Cytotoxic effects of compounds **9**, **14**, and **15** against A) HEK-ACE2, B) MRC-5, and C) Vero E6 cell lines. The cytotoxicity was assessed using the resazurin method. Each data point represents the mean value ± SD of three independent experiments with six replicates each.

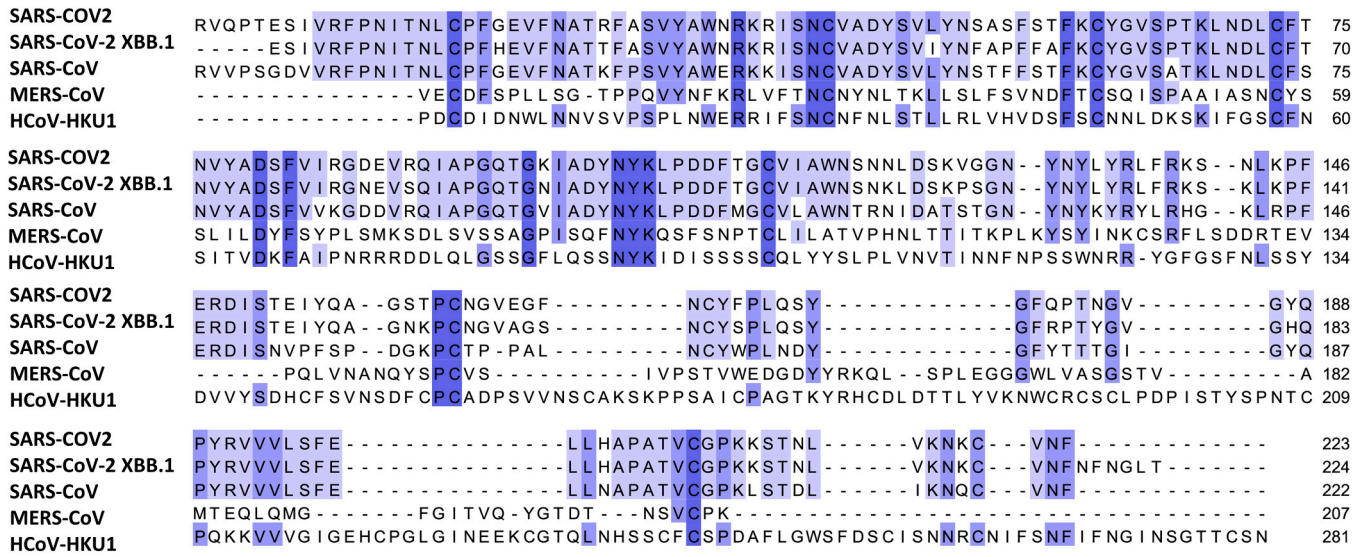

Fig. 5. Sequence alignments of the RBD of spike proteins of SARS-CoV-2, SARS-CoV-2 XBB.1, SARS-CoV-1, MERS-CoV, and HCoV-HKU1. The dark blue color indicates that residues show > 80 % identity with the consensus residues; the blue color indicates > 60 %; the light blue color indicates > 40 %; and the white color indicates < 40 % identity.

nitrile-containing drugs target a variety of diseases such as heart failure, cancer, inflammation, as well as fungal, bacterial, viral infections, and others [28]. Nitrile-containing antiviral drugs were broadly used during the past decades. For instance, etravirine, rilpivirine, and doravirin were employed to inhibit the human immunodeficiency virus (HIV). Remdesivir was first developed for use against the Ebola virus. Since the middle of the year 2020, it has been employed to treat COVID-19 caused by SARS-CoV-2. Nirmatrelvir was developed against SARS-CoV-2 too. The prevalence of nitrile-containing drugs confirms that they may exert better pharmacokinetic and pharmacological effects in comparison to other drugs exhibiting similar therapeutic effects [27].

From the metabolic perspective, the nitrile group is stable and non-toxic, and usually remains unchanged after passing through the human body [29]. Nitrile-containing compounds usually have lower clog *P*-values, which improves their solubilities [28]. Chemically, the nitrile group consists of a nitrogen atom that has a free pair of electrons and is connected to an sp^3-hybridized carbon atom, which gives the nitrile group a linear shape. The molecular volume of the nitrile group is approximately one-eighth the size of the methyl group. This relationship, together with the linear shape, is regarded as a significant factor contributing to the ability of the nitrile group to fit well into binding pockets and to exhibit a high tolerance towards different target mutations.

Natural products and herbal medicines represent a valuable source for drug development [30]. Previous investigations suggest that natural products may provide novel drug candidates against viral infections [31, 32]. Hence, with the aim of finding novel pan-coronaviral compounds we focused on nitrile- and sulfur-containing natural products in this study. We screened a library of 143 sulfur- and nitrile-containing natural products and their derivatives against the RBD of the spike protein of SARS-CoV-2 using AutoDock Vina in the PyRx software package. As a result of this initial screening, the 84 top compounds based on their lowest binding energies were selected and subjected to molecular docking using AutoDock 4.2.6 to validate the virtual screening results. Finally, 18 compounds obtained from the computer-based screening were selected for further *in vitro* experiments. Research on SARS-CoV-2 as a novel human pathogen is restricted to high-level biosafety laboratories, which usually do not have the necessary instrumentation for the large-scale screening of antiviral compounds. Thus, we first used a pseudovirus technology to overcome this challenge and facilitate the screening of active compounds against the viral entry process in a biosafety level 2 laboratory. The pseudovirus inhibition assay revealed that compounds **9**, **14**, and **15** strongly inhibit the cellular pseudovirus entry, with low micromolar IC_{50} values and a high selectivity index of 26.6, 10 and 12.6 respectively. These finding were confirmed using inhibition of live SARS-CoV-2 replication, where the compounds showed inhibition with higher IC_{50} values with the selectivity index of 4.3 and 3.6 for compounds **9** and **14**, likely due to the low titer of pseudovirus compared to the live viruses. It was remarkable that the cell viability assays evidenced that compounds **9**, **14**, and **15** exerted only moderate

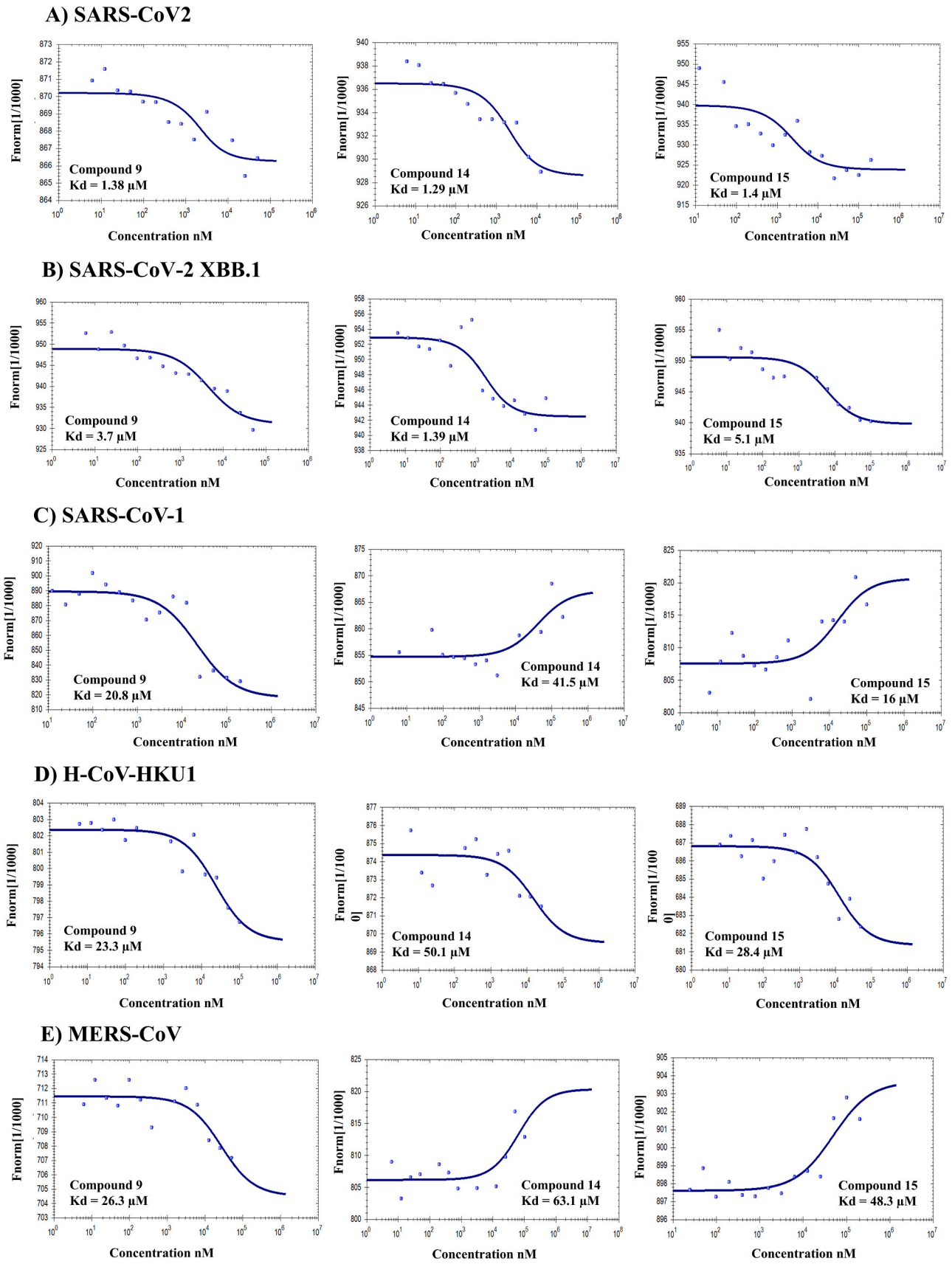

Fig. 6. Microscale thermophoresis analysis of compounds **9**, **14**, and **15** with the RBD of spike protein of: A) SARS-CoV-2, B) SARS-CoV-2 XBB.1, C) SARS-CoV-1, D) H-CoV-HKU1, and E) MERS-CoV.

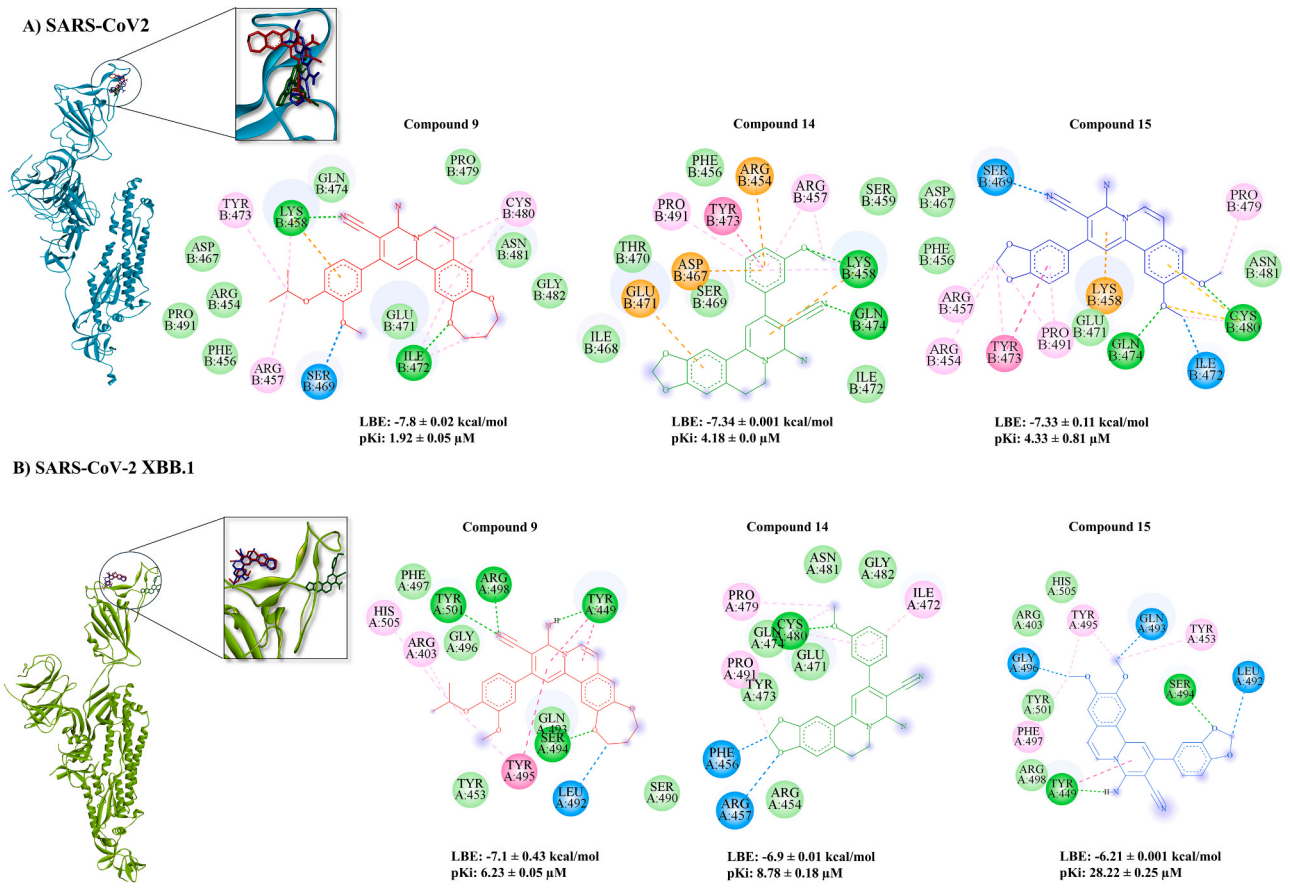

Fig. 7. The binding mode and 2D representation of compounds **9**, **14**, and **15** with the RBD of spike protein of: A) SARS-CoV-2 (PDB ID: 7bnn), B) SARS-CoV-2 XBB.1 (PDB ID: 8iou), C) SARS-CoV1 (PDB ID: 6acd), D) MERS-CoV (PDB ID: 6nb03), and E) HCoV-HKU1 (PDB ID: 8opo). These visualizations were generated using Discovery Studio Visualizer software (version v.24.1.0.23298). The lowest binding energies (LBE) and the predicted inhibition constant (pKi) of each compound were calculated using AutoDock 4.2.6.

cytotoxicity against HEK-ACE2, and slight toxicities were also observed against human fetal MRC-5 lung fibroblasts and Vero E6 cells.

Compounds **9**, **14**, and **15**, as also compound **16**, are structurally related to each other. Among these four compounds, **16** showed the weakest activity (less than 50 % of inhibition). Structurally, it is the only one with an electron-withdrawing group on the phenyl substituent in the "south" (bottom): a carboxymethyl (*i.e.*, a methyl ester) group. A much better activity was found for compound **14**. It has an electron-donating methoxy group (-OMe) on that phenyl substituent in the “south”. This fits significantly with the fact that the two highest activities are exhibited by compounds **9** and **15**, which both have even two electron-donating alkoxy groups on that “southern” phenyl ring. The “north-western” (upper-left) part of the molecule is electronically less differentiated. All four structures have two oxygen functions there. The difference between the two best compounds, **9** and **15**, is given by the alkyl (or alkylidene) substituents on the two oxygens on the left upper side of the molecule, and on the two oxygens on the bottom side. On the left upper (“north-western”) side, compound **9** has a large, 7-membered ring, which is more voluminous than the two methoxy groups on the left upper side of compound **15**. Also, on the “southern” phenyl substituent, the combination of a methoxy and an isopropyloxy group, as in compound **9**, is larger than the small 5-membered methylene acetal ring on the “southern” phenyl ring of compound **15**. Apart from the aspect of mere molecular size, however, these groups are not only voluminous for compound **9** and smaller for compound **15** on both sides, but the larger ones on compound **9** are also more lipophilic in both cases. Thus, it seems that not only the molecular shape influences the inhibitory activity but also the lipophilicity.

Compounds **9**, **14**, **15**, and **16** have more in common than the presence of the mentioned nitrile and alkoxy groups. They are, all of them, tetracyclic (or even pentacyclic in the case of the cyclic ether/acetal in the isoquinoline part) heterocycles, which are generally addressed as fused isoquinolines (more exactly as benzo[*a*]quinolizine-4-imines). They are not natural products as such, but are directly derived from a natural product, *viz.* from the natural alkaloid 1-methyl-6,7-dihydroxy-3,4-dihydroisoquinoline [33,34]or from the respective ethers. From these natural products, they are semi-synthetically built up, in a single step, by reaction with malodinitrile and the respective benzaldehyde. Thus, they are easily available by an efficient, natural product-based one-pot semi-synthesis [35,36]. The parent compound, 1-methyl-6,7-dihydroxy-3,4-dihydroisoquinoline, belongs to a group of catecholic isoquinolines, isolated, *i.a.*, from *Portulaca oleracea* L. (plant family: Portulacaceae), also known as common purslane [37]. This is a cosmopolitan succulent plant with a broad spectrum of bioactivities, among them neuroprotective, anti-inflammatory, anti-cancer, and also anti-viral effects [38]. Plant extracts and polysaccharide fractions of *P. oleracea* have been reported to inhibit the porcine epidemic diarrhea virus (PEDV, α-coronavirus), the porcine rotavirus (Reoviridae, double-stranded RNA virus), the influenza A virus, the hepatitis C virus (HCV, Flaviviridae, single-stranded RNA virus), and the herpes simplex virus 2 (HSV-2, Herpesviridae, double-stranded DNA virus) [39–43]. In a commercial SARS-CoV-2 inhibitor screening assay kit, *P. oleracea* extract also inhibited SARS-CoV-2 [44]. Several isoquinoline alkaloids have been shown to inhibit SARS-CoV-2 [45].

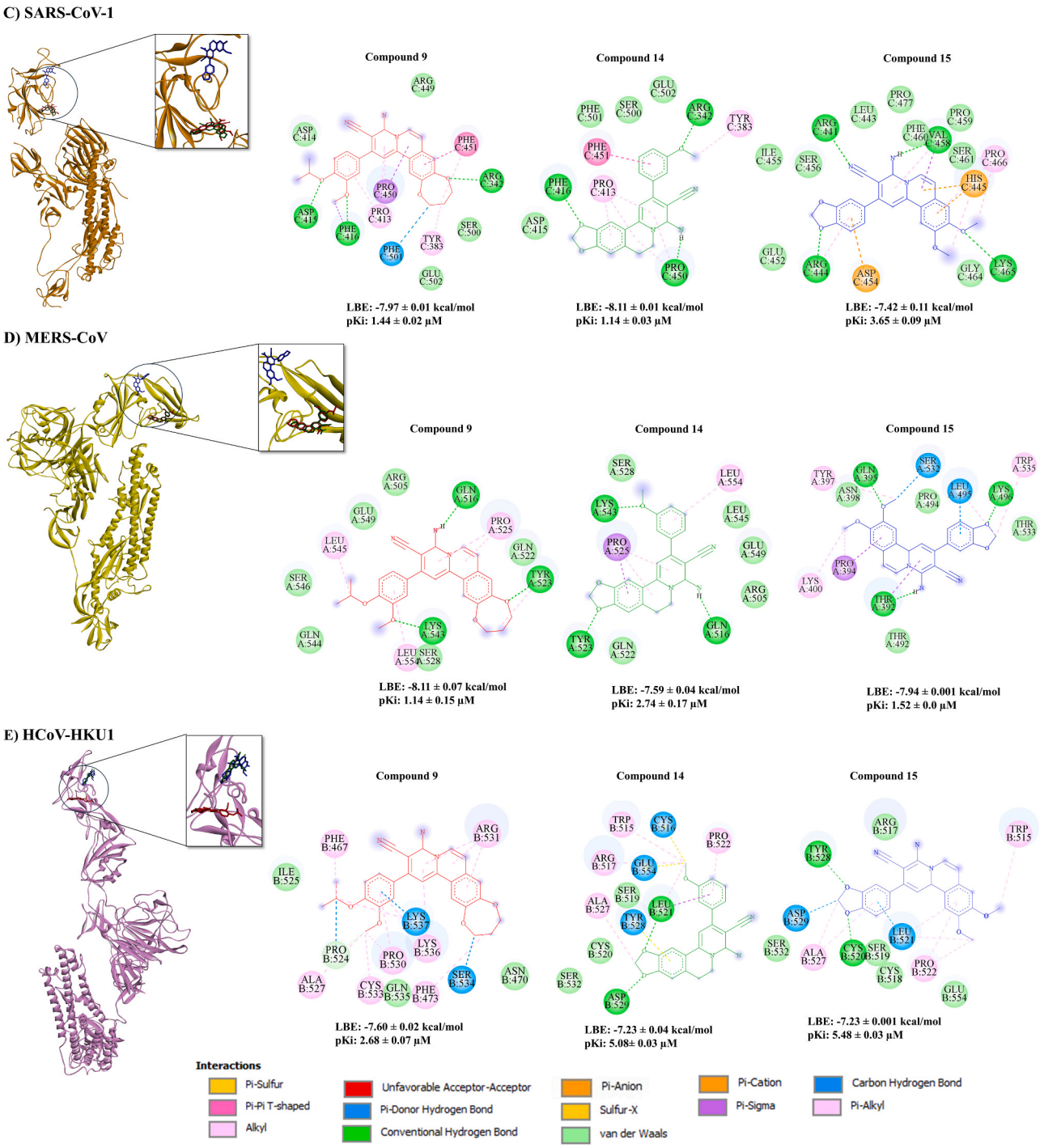

Fig. 7. (*continued*).

To the best of our knowledge, the three active compounds that we identified in the present investigation have not been reported before to inhibit the spike protein in a pseudovirus model of a clinical SARS-CoV-2 isolate. Up to now, numerous investigations have concentrated on the discovery of natural compounds binding to the spike protein of SARS-CoV2 and preventing the viral infection. For instance, H69C2 had a binding affinity (K_d value) of 0.0947 μM for the RBD of SASRS-CoV2 and an inhibitory effect with an IC_{50} value of 85.75 μM against the native live virus [46]. Two organic dyes (Congo red and direct violet 1) were found to bind to the RBD and inhibited pseudovirus entry and cell infection with IC_{50} values of 27.4 and 16.4 μM, respectively, that were higher than the IC_{50} values of compounds **9**, **14**, and **15** [6]. Although different peptides and small molecules were developed as pan-coronavirus inhibitors against the spike protein in the past, they all targeted the fusion peptide of the spike protein and inhibited the cellular entry of coronaviruses through the inhibition of membrane fusion at low micromolar IC_{50} values [47–49].

With the aim of developing a pan-coronaviral inhibitors targeting the RBD domain of the spike protein, we first performed a sequence alignment for the RBD of SARS-CoV2, SARS-CoV-2 XBB.1 (Omicron variant), SARS-CoV-1, MERS-CoV, and HCoV-HKU1. The Omicron variant showed the highest and MERS-CoV the lowest homology to wild-type SARS-CoV-2. We then performed microscale thermophoresis to investigate whether these three active compounds can bind to the RBD of the

spike protein of other coronavirus family members. Indeed, all three active compounds bound to the RBD of the spike protein of SARS-CoV2, SARS-CoV-2 XBB.1, SARS-CoV-1, MERS-CoV, and HCoV-HKU1. Their binding affinities decreased with their sequence homology identified by sequence alignment with a good correlation (R = -0.88, -0.91, -0.93 and *p*-value = 0.04, 0.03, 0.02 for Compounds **9**, **14** and **15** respectively).

According to previous studies, there were some residues on the RBD of SARS-CoV2 considered as hotspot residues for protein-protein or protein-ligand binding, including R402, N439, N440, L441, K433, V444, G446,Y449, Y453, L452, L455, F456, T4790, E471, I472, N481, E484, F486, N487,Y489, F490, Q493, Q498, P499, T500, N501, and Y505 [46, 50]. A pharmacophore analysis based on the docking simulation revealed that compounds **9**, **14**, and **15** interacted with some of these hotspot residues, including F456, T470, E471, and N481. Thus, the compounds may interfere with the interaction between these residues and ACE2. The Omicron and wild-type RBDs shared similar overall structures, while the RBD of Omicron demonstrated higher binding affinity for the ACE2 compared to the wild-type RBD [50]. Our molecular docking analysis revealed that the three active compounds, **9**, **14**, and **15**, interacted with some of the hot spot residues in the RBDs of SARS-CoV2, SARS-CoV-2 XBB.1, *i.e.*, F456, R498, S496, Y501, and H505 that may interfere with the interaction between RBD and ACE2. While previous studies demonstrated that the N501Y mutation allows the virus to escape from monoclonal antibodies, convalescent plasma, and vaccines [46,51], our molecular docking results showed that mutations in this residue do not affect binding of the active compounds **9**, **14**, and **15**. Moreover, molecular docking revealed that compounds **9**, **14**, and **15** may inhibit the HCoV-HKU1 virus entry through the interaction with the R531, R517, Y528, and D529 hotspot residues [52]. Although compounds **9**, **14,** and **15** did not interact with the hotspot residues of SARS-CoV-1 and MERS-CoV, they still exerted high affinities to the RBD based on their LBE of molecular docking and K_d values of microscale thermophoresis studies. Thus, the inhibitory effects of these compounds towards SARS-CoV-1 and MERS-CoV could take place by conformational changes of the RBD [53].

In summary, we report here on a group of nitrile-containing natural product-derived compounds as broad-spectrum coronaviral entry inhibitors with low toxicity. Initially starting with a focus on nitrile- and/or sulfur-containing structures as the prime criterion, our strategy has led to no less than three highly promising and easy-to-synthesize agents, remarkably all of them with nitrile groups, but none with sulfur. Likewise remarkable is the fact that all of them have an isoquinoline-derived structure, despite the broad plethora of the other ZINC-derived starting structures. This shows the efficiency and specificity of the chosen selection pathway, which, out of a very large number of starting structures picks out this promising class of heterocycles. These compounds effectively protect the cells from infection with both SARS-CoV-2 pseudoviruses and live viruses. Moreover, *in silico* and *in vitro* studies revealed that they bind to the RBD of SARS-CoV-2 XBB.1, SARS-CoV-1, MERS-CoV, and HCoV-HKU1 with high affinities. We thus conclude that these compounds may be interesting candidates to develop novel potent pan-coronavirus entry inhibitors, in particular compound **15**, which had the highest antiviral activity. Further investigations including *in vivo* studies are required.

CRediT authorship contribution statement

Sara Abdelfatah: Conceptualization. **Nasim Shahhamzehei:** Writing – review & editing, Writing – original draft, Methodology, Formal analysis, Conceptualization. **Kathrin Sutter:** Methodology. **Hannah S. Schwarzer-Sperber:** Methodology. **Gerhard Bringmann:** Writing – review & editing, Writing – original draft, Conceptualization. **Rümeysa Yücer:** Methodology. **Thomas Efferth:** Writing – review & editing, Conceptualization. **Roland Schwarzer:** Writing – review & editing.

Declaration of Competing Interest

The authors declare that they have no known competing financial interests or personal relationships that could have appeared to influence the work reported in this paper.

Data availability

Data will be made available on request.

Acknowledgement

We are grateful to the financial support of Marc Strobel, Frankfurt a. M., Germany and CVC Philanthropy, Jersey.

Conflict of interest

The authors declare that there is no conflict of interest.

References

[1] J. Zhang, T. Xiao, Y. Cai, B. Chen, Structure of SARS-CoV-2 spike protein, Curr. Opin. Virol. 50 (2021) 173–182, https://doi.org/10.1016/j.coviro.2021.08.010.
[2] S. Xia, L. Wang, Y. Zhu, L. Lu, S. Jiang, Origin, virological features, immune evasion and intervention of SARS-CoV-2 Omicron sublineages, Signal Transduct. Target Ther. 7 (2022), https://doi.org/10.1038/s41392-022-01105-9.
[3] S. Moreno, B. Alcázar, A. Antela, C. Dueñas, J.G. Del Castillo, J. Olalla, Use of antivirals in SARS-CoV-2 infection. Critical review of the role of remdesivir, Drug Des. Dev. Ther. 16 (2022) 827–841, https://doi.org/10.2147/DDDT.S356951.
[4] L.D. Saravolatz, S. Depcinski, M. Sharma, Molnupiravir and nirmatrelvir-ritonavir: oral coronavirus disease 2019 antiviral drugs, Clin. Infect. Dis. 76 (2023) 165–171, https://doi.org/10.1093/cid/ciac180.
[5] M.G. Cox, T.P. Peacock, W.T. Harvey, J. Hughes, D.W. Wright, B.J. Willett, E. Thomson, R.K. Gupta, S.J. Peacock, D.L. Robertson, A.M. Carabelli, SARS-CoV-2 variant evasion of monoclonal antibodies based on in vitro studies, Nat. Rev. Microbiol. 21 (2023) 112–124, https://doi.org/10.1038/s41579-022-00809-7.
[6] D. Bojadzic, O. Alcazar, J. Chen, S.T. Chuang, J.M. Condor Capcha, L.A. Shehadeh, P. Buchwald, Small-molecule inhibitors of the coronavirus spike: ACE2 protein-protein interaction as blockers of viral attachment and entry for SARS-CoV-2, ACS Infect. Dis. 7 (2021) 1519–1534, https://doi.org/10.1021/acsinfecdis.1c00070.
[7] Y. Huang, C. Yang, X. feng Xu, W. Xu, S. wen Liu, Structural and functional properties of SARS-CoV-2 spike protein: potential antivirus drug development for COVID-19, Acta Pharm. Sin. 41 (2020) 1141–1149, https://doi.org/10.1038/s41401-020-0485-4.
[8] C. Zhao, K.P. Rakesh, L. Ravidar, W.Y. Fang, H.L. Qin, Pharmaceutical and medicinal significance of sulfur (SVI)-containing motifs for drug discovery: a critical review, Eur. J. Med. Chem. 162 (2019) 679–734, https://doi.org/10.1016/j.ejmech.2018.11.017.
[9] S. Kim, R. Kubec, R.A. Musah, Antibacterial and antifungal activity of sulfur-containing compounds from Petiveria alliacea L, J. Ethnopharmacol. 104 (2006) 188–192, https://doi.org/10.1016/j.jep.2005.08.072.
[10] L.G. Bahrin, M.O. Apostu, L.M. Birsa, M. Stefan, The antibacterial properties of sulfur containing flavonoids, Bioorg. Med. Chem. Lett. 24 (2014) 2315–2318, https://doi.org/10.1016/j.bmcl.2014.03.071.
[11] O.-G. Nh, F.F. Fleming, Nitrile-containing natural products, n.d.
[12] X. Wang, Y. Wang, X. Li, Z. Yu, C. Song, Y. Du, Nitrile-containing pharmaceuticals: target, mechanism of action, and their SAR studies, RSC Med. Chem. 12 (2021) 1650–1671, https://doi.org/10.1039/d1md00131k.
[13] C. Scotti, J.W. Barlow, Natural products containing the nitrile functional group and their biological activities, Nat. Prod. Commun. 17 (2022), https://doi.org/10.1177/1934578X221099973.
[14] M. Zeino, M.E.M. Saeed, O. Kadioglu, T. Efferth, The ability of molecular docking to unravel the controversy and challenges related to P-glycoprotein – a well-known, yet poorly understood drug transporter, Invest. New Drugs 32 (2014) 618–625, https://doi.org/10.1007/s10637-014-0098-1.
[15] K.H.D. Crawford, R. Eguia, A.S. Dingens, A.N. Loes, J.D. Bloom, K. Crawford, Pseudotyping lentiviral particles with SARS-CoV-2 spike protein for neutralization assays V.2 coronavirus method development community, Viruses (2021), https://doi.org/10.17504/protocols.io.br44m8yw.
[16] S.A. Almahboub, A. Algaissi, M.A. Alfaleh, M.Z. ElAssouli, A.M. Hashem, Evaluation of neutralizing antibodies against highly pathogenic coronaviruses: a detailed protocol for a rapid evaluation of neutralizing antibodies using vesicular stomatitis virus pseudovirus-based assay, Front. Microbiol. 11 (2020), https://doi.org/10.3389/fmicb.2020.02020.
[17] R.K.L. Lee, T.N. Li, S.Y. Chang, T.L. Chao, C.H. Kuo, M.Y.C. Pan, Y.T. Chiou, K. J. Liao, Y. Yang, Y.H. Wu, C.H. Huang, H.F. Juan, H.P. Hsieh, L.H.C. Wang, Identification of entry inhibitors against delta and omicron variants of SARS-CoV-2, Int. J. Mol. Sci. 23 (2022), https://doi.org/10.3390/ijms23074050.
[18] C.S. Heilingloh, U.W. Aufderhorst, L. Schipper, U. Dittmer, O. Witzke, D. Yang, X. Zheng, K. Sutter, M. Trilling, M. Alt, E. Steinmann, A. Krawczyk, Susceptibility

of SARS-CoV-2 to UV irradiation, Am. J. Infect. Control 48 (2020) 1273–1275, https://doi.org/10.1016/j.ajic.2020.07.031.
[19] L. Schöler, V.T.K. Le-Trilling, M. Eilbrecht, D. Mennerich, O.E. Anastasiou, A. Krawczyk, A. Herrmann, U. Dittmer, M. Trilling, A novel in-cell ELISA assay allows rapid and automated quantification of SARS-CoV-2 to analyze neutralizing antibodies and antiviral compounds, Front. Immunol. 11 (2020) 1–11, https://doi.org/10.3389/fimmu.2020.573526.
[20] V. Kuete, A.T. Mbaveng, E.C.N. Nono, C.C. Simo, M. Zeino, A.E. Nkengfack, T. Efferth, Cytotoxicity of seven naturally occurring phenolic compounds towards multi-factorial drug-resistant cancer cells, Phytomedicine 23 (2016) 856–863, https://doi.org/10.1016/j.phymed.2016.04.007.
[21] M. Jerabek-Willemsen, C.J. Wienken, D. Braun, P. Baaske, S. Duhr, Molecular interaction studies using microscale thermophoresis, Assay. Drug Dev. Technol. 9 (2011) 342–353, https://doi.org/10.1089/adt.2011.0380.
[22] E.-J. Seo, T. Efferth, Interaction of antihistaminic drugs with human translationally controlled tumor protein (TCTP) as novel approach for differentiation therapy, Oncotarget (2016). ⟨https://www.impactjournals.com/oncotarget⟩.
[23] M.M. Kesheh, P. Hosseini, S. Soltani, M. Zandi, An overview on the seven pathogenic human coronaviruses, Rev. Med. Virol. 32 (2022), https://doi.org/10.1002/rmv.2282.
[24] X. Lin, X. Li, X. Lin, A review on applications of computational methods in drug screening and design, Molecules 25 (2020) 1–17, https://doi.org/10.3390/molecules25061375.
[25] I. Trifonova, N. Korsun, I. Madzharova, P. Velikov, I. Alexsiev, L. Grigorova, S. Voleva, R. Yordanova, I. Ivanov, T. Tcherveniakova, I. Christova, Prevalence and clinical impact of mono- and co-infections with endemic coronaviruses 229E, OC43, NL63, and HKU-1 during the COVID-19 pandemic, Heliyon 10 (2024) e29258, https://doi.org/10.1016/j.heliyon.2024.e29258.
[26] R. Geng, P. Zhou, Severe acute respiratory syndrome (SARS) related coronavirus in bats, Anim. Dis. 1 (2021) 1–8, https://doi.org/10.1186/s44149-021-00004-w.
[27] X. Wang, Y. Wang, X. Li, Z. Yu, C. Song, Y. Du, Nitrile-containing pharmaceuticals: target, mechanism of action, and their SAR studies, RSC Med. Chem. 12 (2021) 1650–1671, https://doi.org/10.1039/d1md00131k.
[28] X. Wang, Y. Wang, X. Li, Z. Yu, C. Song, Y. Du, Nitrile-containing pharmaceuticals: target, mechanism of action, and their SAR studies, RSC Med. Chem. 12 (2021) 1650–1671, https://doi.org/10.1039/d1md00131k.
[29] V. Bonatto, R.F. Lameiro, F.R. Rocho, J. Lameira, A. Leitão, C.A. Montanari, Nitriles: an attractive approach to the development of covalent inhibitors, RSC Med. Chem. 14 (2022) 201–217, https://doi.org/10.1039/d2md00204c.
[30] B. Chopra, A.K. Dhingra, Natural products: a lead for drug discovery and development, Phytother. Res. 35 (2021) 4660–4702, https://doi.org/10.1002/ptr.7099.
[31] R. Sharma, M. Bhattu, A. Tripathi, M. Verma, R. Acevedo, P. Kumar, V.D. Rajput, J. Singh, Potential medicinal plants to combat viral infections: a way forward to environmental biotechnology, Environ. Res. 227 (2023) 115725, https://doi.org/10.1016/j.envres.2023.115725.
[32] N. Nasim, I.S. Sandeep, S. Mohanty, Plant-derived natural products for drug discovery: current approaches and prospects, Nucleus 65 (2022) 399–411, https://doi.org/10.1007/s13237-022-00405-3.
[33] T.Y. Jin, S.Q. Li, C.R. Jin, H. Shan, R.M. Wang, M.X. Zhou, A.L. Li, L.Y. Li, S.Y. Hu, T. Shen, L. Xiang, Catecholic isoquinolines from portulaca oleracea and their anti-inflammatory and β 2 -adrenergic receptor agonist activity, J. Nat. Prod. 81 (2018) 768–777, https://doi.org/10.1021/acs.jnatprod.7b00762.
[34] X.F. Shang, C.J. Yang, S.L. Morris-Natschke, J.C. Li, X.D. Yin, Y.Q. Liu, X. Guo, J. W. Peng, M. Goto, J.Y. Zhang, K.H. Lee, Biologically active isoquinoline alkaloids covering 2014–2018, Med. Res. Rev. 40 (2020) 2212–2289, https://doi.org/10.1002/med.21703.
[35] L. Li, H. Zhang, M. Zhang, M. Zhao, L. Feng, X. Luo, Z. Gao, Y. Huang, O. Ardayfio, J.H. Zhang, Y. Lin, H. Fan, Y. Mi, G. Li, L. Liu, L. Feng, F. Luo, L. Teng, W. Qi, J. Ottl, A. Lingel, D.E. Bussiere, Z. Yu, P. Atadja, C. Lu, E. Li, J. Gu, K. Zhao, Discovery and molecular basis of a diverse set of polycomb repressive complex 2 inhibitors recognition by EED, PLoS One 12 (2017) 1–18, https://doi.org/10.1371/journal.pone.0169855.
[36] T.A. Abdallah, H.A. Abdelhadi, A.A. Ibrahim, H.M. Hassaneen, Reactivity of 1-methylisoquinoline. One pot synthesis of benzo[a]-quinolizine derivatives, Synth. Commun. 32 (2002) 581–589, https://doi.org/10.1081/SCC-120002405.
[37] Z.Z. Jiao, S. Yue, H.X. Sun, T.Y. Jin, H.N. Wang, R.X. Zhu, L. Xiang, Indoline amide glucosides from Portulaca oleracea: isolation, structure, and DPPH radical scavenging activity, J. Nat. Prod. 78 (2015) 2588–2597, https://doi.org/10.1021/acs.jnatprod.5b00524.
[38] Y.X. Zhou, H.L. Xin, K. Rahman, S.J. Wang, C. Peng, H. Zhang, Portulaca oleracea L.: a review of phytochemistry and pharmacological effects, BioMed Res. Int. 2015 (2015), https://doi.org/10.1155/2015/925631.
[39] C.X. Dong, K. Hayashi, J.B. Lee, T. Hayashi, Characterization of structures and antiviral effects of polysaccharides from Portulaca oleracea L, Chem. Pharm. Bull. 58 (2010) 507–510, https://doi.org/10.1248/cpb.58.507.
[40] S. Noreen, I. Hussain, M.I. Tariq, B. Ijaz, S. Iqbal, Qamar-Ul-Zaman, U.A. Ashfaq, T. Husnain, Portulaca oleracea L. as a prospective candidate inhibitor of hepatitis C virus NS3 serine protease, Viral Immunol. 28 (2015) 282–289, https://doi.org/10.1089/vim.2014.0079.
[41] Y.H. Li, C.Y. Lai, M.C. Su, J.C. Cheng, Y.S. Chang, Antiviral activity of Portulaca oleracea L. against influenza A viruses, J. Ethnopharmacol. 241 (2019) 112013, https://doi.org/10.1016/j.jep.2019.112013.
[42] Y. Liu, L. Zhao, Y. Xie, Z. Chen, S. Yang, B. Yin, G. Li, H. Guo, S. Lin, J. Wu, Antiviral activity of Portulaca oleracea L. extracts against porcine epidemic diarrhea virus by partial suppression on myd88/NF-κb activation in vitro, Microb. Pathog. 154 (2021) 104832, https://doi.org/10.1016/j.micpath.2021.104832.
[43] X. Zhou, Y. Li, T. Li, J. Cao, Z. Guan, T. Xu, G. Jia, G. Ma, R. Zhao, Portulaca oleracea L. polysaccharide inhibits porcine rotavirus in vitro, Animals 13 (2023), https://doi.org/10.3390/ani13142306.
[44] D.A. Al-Quwaie, A. Allohibi, M. Aljadani, A.M. Alghamdi, A.A. Alharbi, R.S. Baty, S.H. Qahl, O. Saleh, A.O. Shakak, F.S. Alqahtani, O.S.F. Khalil, M.T. El-Saadony, A. M. Saad, Characterization of Portulaca oleracea whole plant: evaluating antioxidant, anticancer, antibacterial, and antiviral activities and application as quality enhancer in yogurt, Molecules 28 (2023), https://doi.org/10.3390/molecules28155859.
[45] M. Valipour, A. Hosseini, A. Di Sotto, H. Irannejad, Dual action anti-inflammatory/antiviral isoquinoline alkaloids as potent naturally occurring anti-SARS-CoV-2 agents: a combined pharmacological and medicinal chemistry perspective, Phytother. Res. 37 (2023) 2168–2186, https://doi.org/10.1002/ptr.7833.
[46] L. Wang, Y. Wu, S. Yao, H. Ge, Y. Zhu, K. Chen, W. zhang Chen, Y. Zhang, W. Zhu, H. yang Wang, Y. Guo, P. xiang Ma, P. xuan Ren, X. lei Zhang, H. qiong Li, M.A. Ali, W. qing Xu, H. liang Jiang, L. ke Zhang, L. li Zhu, Y. Ye, W. juan Shang, F. Bai, Discovery of potential small molecular SARS-CoV-2 entry blockers targeting the spike protein, Acta Pharm. Sin. 43 (2022) 788–796, https://doi.org/10.1038/s41401-021-00735-z.
[47] L. Guo, S. Lin, Z. Chen, Y. Cao, B. He, G. Lu, Targetable elements in SARS-CoV-2 S2 subunit for the design of pan-coronavirus fusion inhibitors and vaccines, Signal Transduct. Target Ther. 8 (2023), https://doi.org/10.1038/s41392-023-01472-x.
[48] Q. Lan, L. Wang, F. Jiao, L. Lu, S. Xia, S. Jiang, Pan-coronavirus fusion inhibitors to combat COVID-19 and other emerging coronavirus infectious diseases, J. Med. Virol. 95 (2023), https://doi.org/10.1002/jmv.28143.
[49] S. Xia, L. Yan, W. Xu, A.S. Agrawal, A. Algaissi, C.T.K. Tseng, Q. Wang, L. Du, W. Tan, I.A. Wilson, S. Jiang, B. Yang, L. Lu, A pan-coronavirus fusion inhibitor targeting the HR1 domain of human coronavirus spike, Sci. Adv. 5 (2019), https://doi.org/10.1126/sciadv.aav4580.
[50] J. Lan, X. He, Y. Ren, Z. Wang, H. Zhou, S. Fan, C. Zhu, D. Liu, B. Shao, T.Y. Liu, Q. Wang, L. Zhang, J. Ge, T. Wang, X. Wang, Structural insights into the SARS-CoV-2 omicron RBD-ACE2 interaction, Cell Res. 32 (2022) 593–595, https://doi.org/10.1038/s41422-022-00644-8.
[51] D. Hattab, M.F.A. Amer, Z.M. Al-Alami, A. Bakhtiar, SARS-CoV-2 journey: from alpha variant to omicron and its sub-variants, Infection 2 (2024), https://doi.org/10.1007/s15010-024-02223-y.
[52] L. Xia, Y. Zhang, Q. Zhou, Structural basis for the recognition of HCoV-HKU1 by human TMPRSS2, Cell Res. (2024), https://doi.org/10.1038/s41422-024-00958-9.
[53] S.R. Tzeng, C.G. Kalodimos, Protein activity regulation by conformational entropy, Nature 488 (2012) 236–240, https://doi.org/10.1038/nature11271.